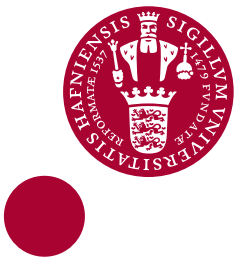

Effects of Cr3+ concentration on the optical properties of Cs2NaAlF6 single crystals

S. Pedro, Sandra; P. Sosman, Lilian ; B. Barthem, Ricardo; C.G. Tedesco, Julio; Bordallo, Heloisa N.

Published in:
Journal of Luminescence

DOI:
10.1016/j.jlumin.2012.09.005

Publication date:
2013

Document version
Publisher's PDF, also known as Version of record

Journal of Luminescence 134 (2013) 100–106

Contents lists available at SciVerse ScienceDirect

Journal of Luminescence

journal homepage: www.elsevier.com/locate/jlumin

Effects of Cr^{3+} concentration on the optical properties of Cs_2NaAlF_6 single crystals

Sandra S. Pedro [a,b,*], Lilian P. Sosman [a], Ricardo B. Barthem [c], Julio C.G. Tedesco [d], Heloisa N. Bordallo [e]

[a] Instituto de Física, Universidade do Estado do Rio de Janeiro, Rua São Francisco Xavier 524, Rio de Janeiro 20559-900, RJ, Brazil
[b] Instituto de Física, Universidade Federal Fluminense, Av. Gal. Milton Tavares de Souza, s/no. — Campus da Praia Vermelha, CEP 24210-346, Niterói, RJ, Brazil
[c] Instituto de Física, Universidade Federal do Rio de Janeiro, Cidade Universitária, Ilha do Fundão, Rio de Janeiro 21941-972, RJ, Brazil
[d] Instituto de Física, Universidade Estadual de Campinas, Cidade Universitária Zeferino Vaz, Campinas 13083-859, SP, Brazil
[e] Niels Bohr Institute, University of Copenhagen, Universitetsparken 5, 2100 Copenhagen, Denmark

ARTICLE INFO

Article history:
Received 3 May 2012
Received in revised form
27 August 2012
Accepted 5 September 2012
Available online 15 September 2012

Keywords:
Luminescence
Optical properties
Insulators
Single crystal

ABSTRACT

This work is devoted to the study of optical properties of the elpasolite Cs_2NaAlF_6 with 0.1, 1.0, 3.0, 10.0, 30.0 and 50.0% of Cr^{3+} ions. The interest in this system lies on the fact that it presents a high quantum yield in the visible and infrared regions and therefore can be considered for laser applications. The photoluminescence and excitation spectra were obtained at 5 and 300 K, while the absorption spectra were measured at 300 K. The spectra at 300 K show broad bands attributed to the Cr^{3+} ions in two non-equivalent sites, both of them with octahedral coordination, while at 5 K we can observe the vibrational modes of the $[CrF_6]^{3-}$ complex. The ensemble of our results lead us to conclude that the material has potential applications as a lasing system.

1. Introduction

In the last years a growing interest in the development of new insulating materials doped with transition metals has been observed, leading these materials to be applied in a wide range of fields, for instance, as signal transmission [1], displays manufacturing [2], tunable solid state lasers at room temperature [3], optical sensors [4], electroluminescent and thermoluminescent devices [5,6], broadband amplifiers [7], radiation detectors [8], white-light emission sources [9,10] and many other areas. These compounds also present very interesting optical properties, such as emission in a wide spectrum with high quantum yield, broad absorption bands and high emission intensity. These optical properties are originated from the coupling between electronic transitions and vibrational modes around the impurity ion. In materials doped with Cr^{3+} ion these broad bands are caused by the transitions between energy levels with $3d^3$ electronic configuration [1]. In general, these systems are attractive because the transitions occur in the visible and infrared regions, if the ions are in octahedral sites [1], or only in the infrared region, if ions are in tetrahedral sites [11]. As fluoride systems doped with transition metals have these properties, they are promising materials for use in the applications mentioned above [12–16].

When a Cr^{3+} ion is surrounded by ligand anions, its energy levels are modified by crystal field due to the potential generated by ligands at the Cr^{3+} position. Using Tanabe-Sugano diagrams [17,18] these new energy levels can be well described. Thus, considering a low crystal field, the fundamental energy level ^4F splits into $^4A_2(t_2^3)$ fundamental level and $^4T_2(t_2^2e)$ and $^4T_1(t_2^2e)$ excited levels. The first excited level, ^4P, becomes the $^4T_1(t_2e^2)$ level and the ^2G level splits into $^2E(t_2^3)$, $^2T_1(t_2^3)$, $^2T_2(t_2^3)$ and $^2A_1(t_2^2e)$ levels. Furthermore, transitions between states with the same spin multiplicity are allowed generating intense bands in the optical spectra, while transitions between different spin multiplicities are forbidden and associated with weak bands [19]. In addition, broad bands are produced by transitions between energy levels with different electronic configurations, while narrow bands are generated by transitions between levels with the same electronic configuration [19]. Therefore, for Cr^{3+} ions the transitions $^4A_2(t_2^3) \leftrightarrow {}^4T_1(t_2^2e)$ or $^4A_2(t_2^3) \leftrightarrow {}^4T_2(t_2^2e)$ produce wide and intense bands, while transitions between the $^4A_2(t_2^3)$ and $^2E(t_2^3)$, $^2T_1(t_2^3)$, $^2T_2(t_2^3)$ or $^2A_1(t_2^2e)$ levels generate narrow and weak bands. In this paper we have performed an extensive study of the optical properties of the elpasolite Cs_2NaAlF_6, complementing previous works of the other authors about the energy levels [20], EPR experiments [21,22], absorption and emission [23], and quantum efficiency of the system by photoacoustic spectroscopy [24].

The system Cs_2NaAlF_6 crystallizes in a hexagonal elpasolite structure, with lattice parameters given by $a=6.176$ Å and $c=29.819$ Å, where the Na^+ and Al^{3+} cations are octahedrally

* Corresponding author. Present address: Instituto de Física, Universidade Federal Fluminense, Av. Gal. Milton Tavares de Souza, s/no. — Campus da Praia Vermelha, CEP 24210-346, Niterói, RJ, Brazil. Tel.: +55 21 8769 1268.
E-mail address: sspedro@if.uff.br (S.S. Pedro).

0022-2313/$ - see front matter © 2012 Elsevier B.V. All rights reserved.
http://dx.doi.org/10.1016/j.jlumin.2012.09.005

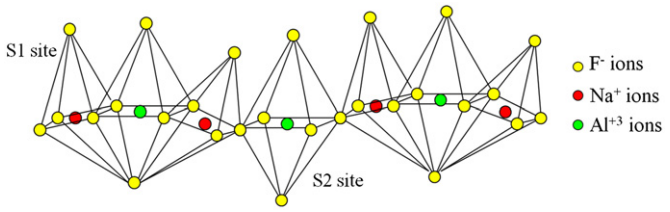

Fig. 1. Diagram of two octahedral sites available for Cr^{3+} occupation in replacement the Al^{3+} ions. The S1 sites represent octahedra linked by faces and the S2 sites represent octahedra linked by corners. The yellow circles represent the fluorine ions, the red circles represent the sodium ions and the green circles are the aluminum ions, where the Al^{3+} positions can be occupied by the Cr^{3+} ions inserted in the crystalline lattice. (For interpretation of the references to color in this figure legend, the reader is referred to the web version of this article.)

surrounded by F^- anions [25,26]. When doped with 0.5% of Cr^{3+} interesting optical properties have been reported [14,23]. Considering the ionic radii and valence of Cr^{3+} (0.64 Å), Na^+ (0.98 Å) and Al^{3+} (0.57 Å) ions, it can be inferred that the replacement of Al^{3+} by Cr^{3+} ions is more likely [13]. Indeed, based on X-ray and neutron diffraction [27] and photoluminescence measurements for this system [14], such assumption was confirmed. Moreover, it was shown that the incorporation of Cr^{3+} in Cs_2NaAlF_6 induces local distortions, without however modifying the host structure, which possesses two nonequivalent octahedral sites of Al^{3+} that are occupied by Cr^{3+} ions [14,21,22,27,28]. As shown in Fig. 1, one of these sites, hereafter called S1, is composed by (AlF_6) octahedral units linked to two (NaF_6) units by faces, while the other site, hereafter S2, is composed by one octahedron (AlF_6) connected to two S1 sites through corners [14,21,27,28]. Neutron diffraction experiments realized with the 0.5 at% sample [27] showed that the metal–ligand distances between Al–F ions are 1.8189(5) Å and 1.8304(5) Å for S1 and S2 sites, respectively. Although some authors assume that the *Dq* parameter depends on $R^{-4.5}$ [29–31], in this work we consider that the *Dq* value depends on R^{-5}, where R is the distance impurity–ligand [17–19]. Nevertheless in both approaches, the site with the shortest metal impurity–ligand distance will present the strongest crystalline field. Therefore, we expect that when the Cr^{3+} ion occupies the S1 site, the crystal field intensity will be higher than on Cr^{3+} ion at S2 site.

The aim of this work is to get insight on the evolution of the optical properties of the host system as a function of the Cr^{3+} concentration. Such properties were carefully investigated by photoluminescence, excitation and optical absorption. From the obtained results on Cs_2NaAlF_6 single crystals doped with 0.1, 1.0, 3.0, 10.0, 30.0 and 50.0 at% of Cr^{3+} replacing Al^{3+} ions, we were able to establish a correlation between the optical and structural properties of this material.

2. Material and methods

2.1. Samples

The samples used in this work were grown by hydrothermal method [14,32]. Single crystals of $Cs_2NaAl_{1-x}Cr_xF_6$ with the nominal concentrations x=0.001, 0.01, 0.03, 0.1, 0.3 and 0.5 were prepared. The fluorides were synthesized by a direct temperature-gradient method as a result of the reaction of aqueous solutions of CsF (30–35 mol%) and NaF. The oxides Al_2O_3 and Cr_2O_3 were added to the aqueous solution at a temperature about 750 K, with a temperature gradient of 2 K/cm and pressures of 100–150 MPa. For these experiments, autoclaves with copper liners having a volume of about 40 cm^3 were used. Under these conditions, were obtained nucleated crystals up to 0.5 cm^3 in size.

2.2. Optical measurements

Luminescence and excitation measurements at 300 K were performed using a 1 kW Xenon lamp (with a monochromator) and a He–Ne laser (14 mW, 632.8 nm) as excitation sources, modulated with variable speed choppers (PAR 191 and SR-540). Emission scan were obtained using spectrometers 2061 McPherson and SPEX 1702. The signal was detected with photomultipliers (RCA 31034 and Hamamatsu R943-02). Lock-in (EG&G PAR 5209 and EG&G 5210) and a digital oscilloscope (Tektronix TDS 350) were used to acquire and process the signal. Absorption data were obtained with a CAM SPEC M 330 UV–vis spectrometer. Optical measurements at 5 K were acquired with an optical He flow cryostat Janis STVP-100.

3. Results and discussion

Fig. 2 shows the photoluminescence spectra at 300 K of the Cs_2NaAlF_6 system with 0.1, 1.0, 3.0, 10.0, 30.0 and 50.0 at% of Cr^{3+} obtained with 632.8 nm excitation modulated at 102 Hz. The intense and broad bands were observed at the red-infrared region and attributed to the spin-allowed transition $^4T_2(^4F)\rightarrow{}^4A_2(^4F)$ of Cr^{3+} ions in octahedral sites [14,23]. The inhomogeneous broadening of the bands is an evidence of the existence of two nonequivalent Cr^{3+} sites [14,27].

Moreover, from these spectra it is possible to obtain information of how the impurity concentration influences the luminescence. Therefore, the integrated intensity and band barycenter were extracted from the spectra and are shown in Fig. 3. The decrease of the luminescence integrated intensity with concentration (Fig. 3(b)) is due to the photon absorption emitted by the Cr^{3+} ions to their first neighbors [33]. On the other hand, the shift of the maximum of the photoluminescence energy band to lower values (longer wavelengths) is noticed with the increase of the impurity concentration up to 10.0% (Fig. 3(a)). A similar effect was also observed in $ZnAl_{2(1-x)}Cr_{2x}S_4$ single crystals [34]. The observed phenomena can be explained of the following way: when the concentration increases the Cr^{3+} ions tend to be in closer

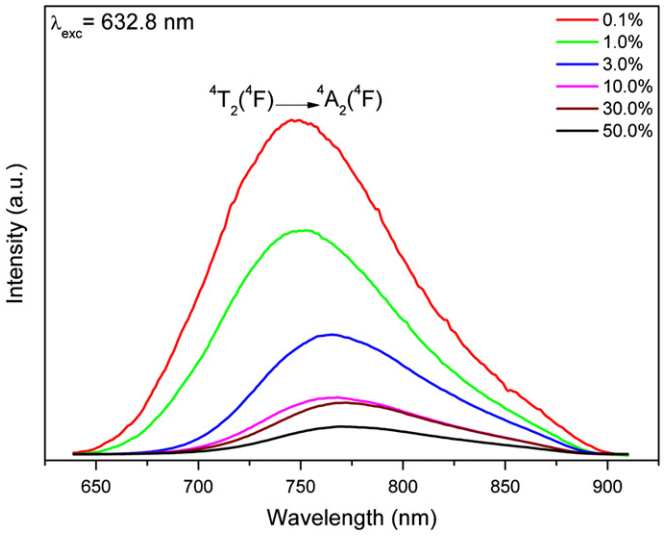

Fig. 2. Photoluminescence spectra at 300 K of Cs_2NaAlF_6, with 0.1, 1.0, 3.0, 10.0, 30.0 and 50.0 at% of Cr^{3+}. (For interpretation of the references to color in this figure legend, the reader is referred to the web version of this article.)

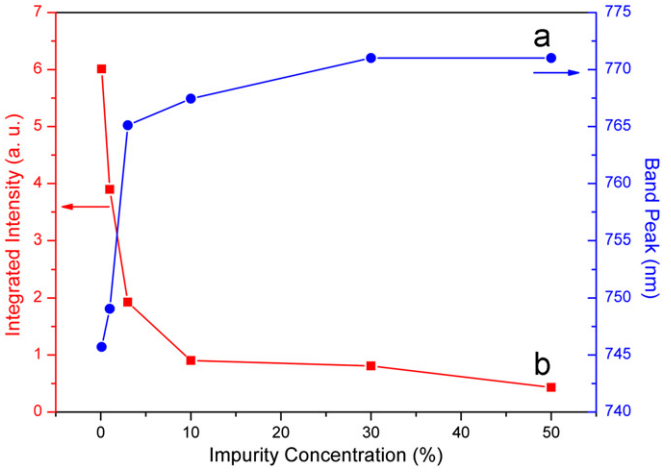

Fig. 3. (a) Band peak and (b) integrated intensity as function of Cr^{3+} impurity concentration.

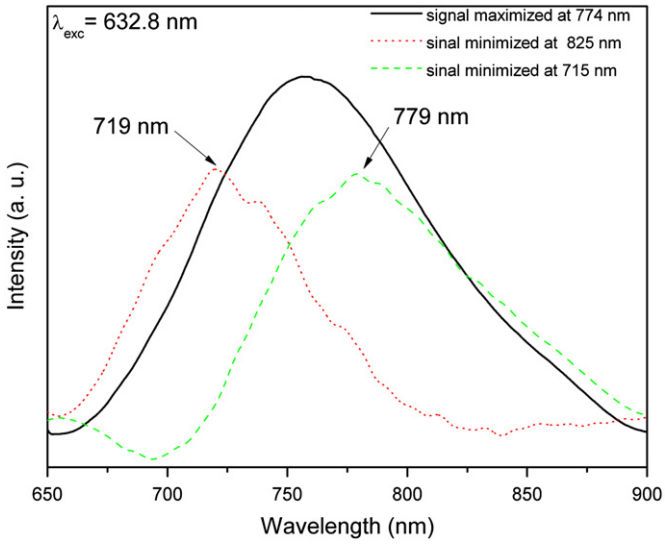

Fig. 4. Cs_2NaAlF_6 luminescence spectra at 300 K with 0.1 at% of Cr^{3+}. (For interpretation of the references to color in this figure legend, the reader is referred to the web version of this article.)

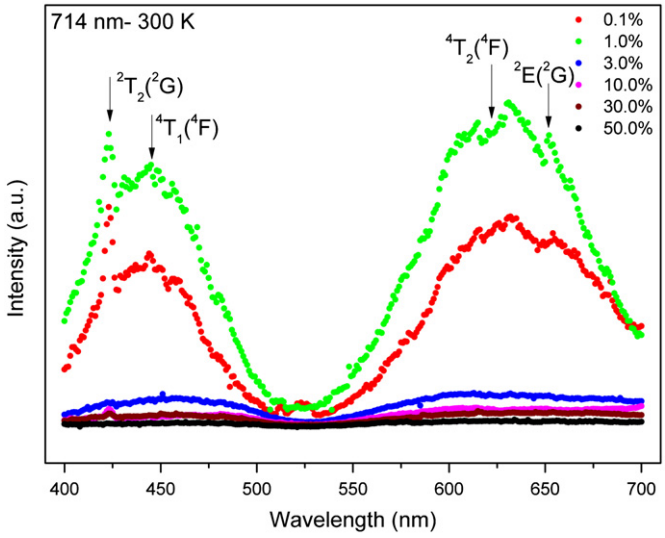

Fig. 5. Excitation spectra at 714 nm (300 K) of the Cs_2NaAlF_6 with several concentrations of the Cr^{3+} ion. The identified transitions are labeled in the spectra.

proximity, and as a result the neighboring ions will tend to absorb the emitted radiation from each other. In addition, considering that from the Tanabe-Sugano energy level diagrams for d^3 configuration [17–19], the energy of the $^4T_2(^4F)$ state increases with increasing the crystal field parameter *Dq*, as already discussed in the Introduction, the transitions that occur at higher energy regions are assigned to the S1 site, while the transitions occurring in lower energy regions to the S2 site [14,27]. As we can infer from neutron diffraction data from the 0.5% doped sample [27], a difference of approximately 1% in the metal–ligand distance, between the S1 and S2 sites is observed. This small difference can be reflected upon the optical results, as will be seen later. In addition, from Raman data published for several concentrations [27,35], it is observed that the Raman active bands are the same for the whole concentration range, thus implying that not only the average but also the local crystal structure is maintained, and the assumption of different sites is valid in the whole concentration range.

In a more detailed analysis of data presented in Fig. 2, we note that the spectrum for the 0.1% sample has the broadest band. To better resolve this signal, further measurements at 300 K were performed, using the 632.8 nm line of a He–Ne laser. The result is shown in Fig. 4. By maximizing the signal at the lock-in at 774 nm the black curve (full line) was obtained, while by minimizing the signal at 715 nm (green dashed line) and 825 nm (red dotted line) we obtained bands with a maximum emission at 779 and 719 nm, respectively. This photoluminescence signal indeed originates from two different Cr^{3+} octahedral sites. As the bands were not completely separated, we can argue that the transitions are strongly overlapped.

Using the time-resolved luminescence method, the τ_R radiative decay time (or radiative lifetime) was obtained. We observed that the luminescence decreases exponentially with the time for all samples, as typically seen on spectra of isolated impurities [33]. From these results we obtained $\tau_R = 310(8)$ μs for the 1.0% sample and $\tau_R = 181(4)$ μs for the 50.0% sample. A lower radiative time is related to a higher transition probability, and in turn to a lower symmetry. Therefore, the increase of Cr^{3+} concentration induces distortions in the sites occupied by Cr^{3+} ions. Moreover, as the non-radiative transitions become more competitive at higher concentrations, the intensity of luminescence decreases reducing radiative lifetime.

In an attempt to separate the emissions of the two sites, we performed excitation measurements in the high and low energy regions. The excitation spectra at 300 K are shown in Figs. 5 and 6 for all samples at 714 and 780 nm, respectively. It can be observed that all excitation spectra presented the same shape, typical of Cr^{3+} in octahedral site. However, the spectra with higher concentrations (above 1.0%) have much lower intensity. In order to analyze the data, two Gaussian curves were adjusted to the spectra and their barycenter energy values were identified as $^4A_2(^4F) \rightarrow {}^4T_1(^4F)$ and $^4A_2(^4F) \rightarrow {}^4T_2(^4F)$ electronic transitions [17,18]. Additionally, we can see a sharp line overlapped to higher energy band in the 714 nm excitation, which was attributed to the $^4A_2(^4F) \rightarrow {}^2T_2(^2G)$ electronic transition. The structure observed in the lower energy band was estimated as the $^4A_2(^4F) \rightarrow {}^2E(^2G)$ electronic transition. The excitation spectra shapes are clear evidences that Cr^{3+} was incorporated as impurity in the host system and according the luminescence results contribution of two sites are seen. However, here again we observe that the transitions are strongly overlapped. Moreover, the signal–noise ratio is not completely favorable. Therefore is very difficult to obtain exact values for the energy parameters, so the obtained values are approximate.

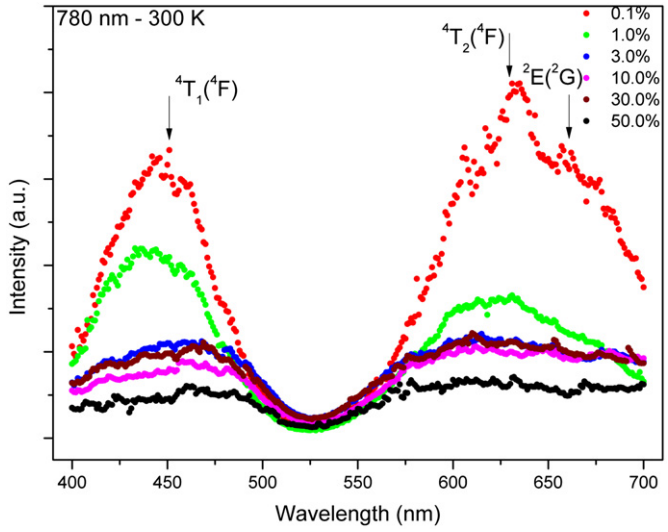

Fig. 6. Excitation spectra at 780 nm (300 K) of the Cs_2NaAlF_6 with several concentrations of the Cr^{3+} ion. The identified transitions are labeled in the spectra.

Table 1
Calculated crystal field parameters for the 0.1% and 1.0% samples for emission excitations at 714 and 780 nm, at 300 K. The Racah parameter *C* was not calculated for the 1.0% sample because the corresponding transition was not identified in the 780 nm excitation spectra.

0.1% Sample	**714 nm**	**780 nm**
Dq (cm^{-1})	1570	1560
B (cm^{-1})	735	713
C (cm^{-1})	3312	3336
Dq/*B*	2.14	2.19
1.0% Sample	**714 nm**	**780 nm**
Dq (cm^{-1})	1590	1587
B (cm^{-1})	694	698
C (cm^{-1})	3409	–
Dq/*B*	2.29	2.28

From the energy values of the transitions obtained from the excitation spectra at 300 K, we calculated the values of the crystal field *Dq* and Racah *B* and *C* parameters according to the next equations [33] for the 0.1% and 1.0% samples, where ΔE is the energy difference between $^4T_1$ and $^4T_2$ levels:

$$E\left(^4T_2\right) = 10Dq \tag{1}$$

$$\frac{B}{Dq} = \frac{(\Delta E/Dq)^2 - 10(\Delta E/Dq)}{15((\Delta E/Dq) - 8)} \tag{2}$$

$$\frac{E(^2E)}{B} \simeq 3.05\frac{C}{B} + 7.90 - 1.80\frac{B}{Dq} \tag{3}$$

The obtained values at 714 and 780 nm excitations are showed at Table 1. These values are characteristic of the Cr^{3+} ion in octahedral coordination, and the ratio $Dq/B = 2.14$ (714 nm excitation) and 2.19 (780 nm excitation) for the 0.1% sample indicates an intermediate crystal field, as seen in previous works [14,23]. It was not possible to calculate the crystal field parameters for the other samples, due their low emission intensity. The values found for the parameters *B* and *C*, below the value for the free ion, 918 and 3850 cm^{-1}, respectively [36], indicate that the impurity–ligand bond presents a more covalent than ionic character. In addition, the crystal field parameter *Dq* is higher for the 714 nm excitation and the increase of the *Dq* value is an evidence of decrease of the impurity–ligand distance. However, is important to emphasize that due to the strong overlapping between the emission bands, the bands are reasonable approximations to distinct emissions from both inequivalent Cr^{3+} sites. Thus, the calculated spectroscopic parameters obtained are to be taken as mean values only.

Considering the R^{-5} dependence, as discussed previously, the site with the lower ligand impurity distance will be responsible for the emission in the high energy region for d^3 configuration, thus we can assume that the emission at 714 nm is assigned to the S1 site and the emission at 780 nm is due the S2 site. We can observe that the difference between the *Dq* values is small (about 1%). However, the difference between the distances metal–ligand for the sites is also about 1% (as mentioned early, from neutron diffraction data [27]), reinforcing our assignments. Besides, based on calculations using the exchange charge model (ECM) [20] as well as in EPR experiments [21] we can infer that our assumption is correct. In [20], using the spectroscopy data reported in [14] and from the exchange charge model (ECM), the crystal field parameters were successfully modeled to the energy level structure of the Cr^{3+} using two non-equivalent sites for Cs_2NaAlF_6. The EPR data [21] reported on the existence of two non-equivalent sites, named M2 (labeled in our work as S1) and M1 (labeled by us as S2), and stated that the axial component of the crystal field at site M1 (our S2 site) is smaller than at site M2 (our S1 site).

Here we would like to point out that our interpretation can be extended to the full Cr^{3+} doping range because based on Raman data published for concentrations of 0.1, 0.5, 1.0 and 3.0 at% of Cr^{3+} [27,35], it was shown that the active modes are the same for this low-concentration range, thus implying that not only the average but also the local crystal structure is maintained. Besides, this conclusion is further supported by EPR results, another technique extremely sensitive to tiny changes in the structure of an impurity center, which further proved that the incorporation of Cr^{3+} in Cs_2NaAlF_6 did not cause sizeable structural changes in the host lattice [21,22]. Finally, analysis of the crystal field levels using the exchange charge model (ECM) [20] confirms that the assumption taken to explain our experimental findings is indeed correct.

Now we turn to the discussion on the absorption spectra at 300 K depicted in Fig. 7. In these spectra the two bands observed at 452 and 672 nm are associated to the $^4A_2(^4F) \rightarrow {}^4T_1(^4F)$ and $^4A_2(^4F) \rightarrow {}^4T_2(^4F)$ electronic transitions, respectively. No relevant changes were seen in the shape or in barycenter of the absorption bands with the increasing of the doping level. However, an overlap of the emission and absorption bands was clearly noted. This fact induces an energy transfer between Cr^{3+} ions, leading to a lowering of the luminescence intensity at higher energy region, as observed in Fig. 2. This overlapping can be associated with the shift of luminescence bands to lower energy regions when the concentration of Cr^{3+} increases.

The emission spectra of the sample with 0.1 at% of Cr^{3+} measured at 5 K with the 632.8 nm excitation is shown in Fig. 8. In both spectra we can notice a broad band in the infrared region due to the $^2E(^2G) \rightarrow {}^4A_2(^4F)$ electronic transition [13] overlapped to several sharp lines, identified as $[CrF_6]^{3-}$ vibrational modes [12,13,37–40]. In these experiments, we have used the phase-shift method [41] in order to identify the zero phonon transitions for both Cr^{3+} sites [13]. Fig. 8(a) shows the spectrum obtained with the zero phonon line maximized at 672 nm, and in Fig. 8(b) the spectrum was measured with the zero phonon line at 672 nm[1] (14870 cm^{-1}) minimized,

[1] The energy of a transition is estimated by the wavelength where the transition occurs. In Spectroscopy, the relation between energy (E) and wavelength (λ) is given by $E\ (cm^{-1}) = 10^7/\lambda\ (nm)$.

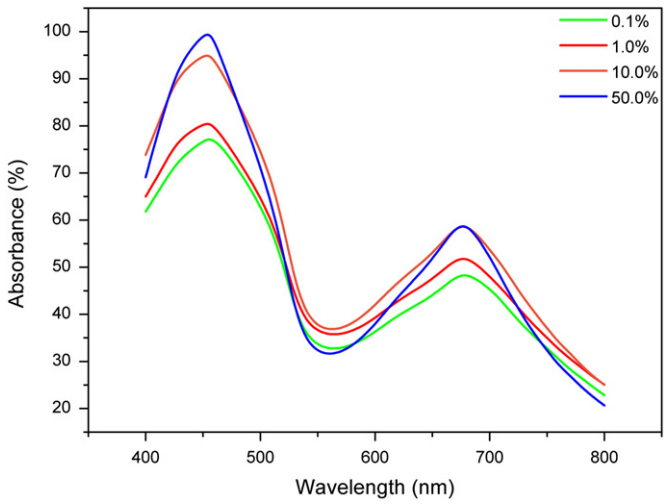

Fig. 7. Absorption spectra at 300 K of the Cs_2NaAlF_6 with the concentrations of 0.1, 1.0, 10.0 and 50.0 at% of Cr^{3+}.

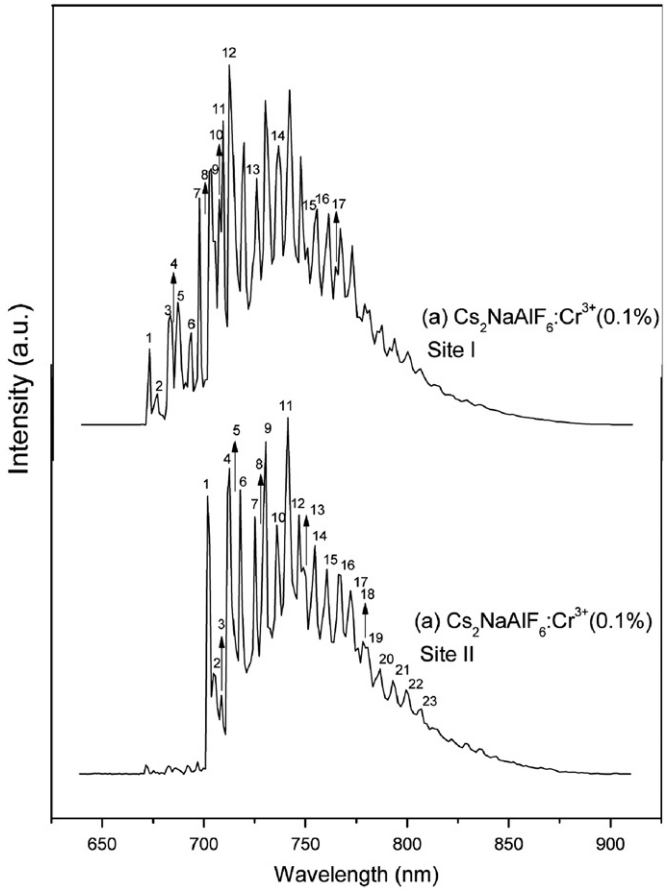

Fig. 8. Emission spectra of the Cs_2NaAlF_6 with 0.1 at% of Cr^{3+} as impurity at 5 K. (a) Spectrum obtained with 672 nm zero-phonon line maximized and in (b) with the line minimized at 672 nm.

where it is observed a new zero phonon line in a different position at lower energy (14250 cm^{-1}, 702 nm). However, as in this region, the ^2E and $^4T_2$ levels are very close, the emission might also be attributed to a mixture between these levels [13]. Thus the multi-phonon nature of the sideband accompanying the zero phonon transition could be taken as a possible evidence of this overlapping, and may contain a significant contribution due the $^4T_2 \rightarrow {}^4A_2$ transition. As a result, and considering that the relaxation from the $^4T_2$ energy level dominates the emission spectra, we can argue that the energy of the relaxed $^4T_2$ state is approximately midway between the energies of the $^4A_2 \rightarrow {}^4T_2$ excitation band and the $^4T_2 \rightarrow {}^4A_2$ emission band. Accordingly, for the center with the higher energy emission peaking at 719 nm (14,908 cm^{-1}), and associated to the S1 site (Fig. 4), such a calculation yields a value of about 675 nm (14,803 cm^{-1}), which is very close to the wavelength of the zero phonon line of the higher energy emission, located at 672 nm (14,870 cm^{-1}). For the S2 site with an emission band at 779 nm (12,840 cm^{-1}) the calculated value of 703 nm (14,210 cm^{-1}) is also very close to the value of the zero phonon line of 702 nm (14,250 cm^{-1}). This interpretation would also lead to the conclusion that the energy of the relaxed $^4T_2$ state is larger for the higher energy emission than for the lower energy emission, in full agreement with our results as well. Without any doubt, the results present here are yet another evidence of two-site occupation by the Cr^{3+} impurity ions [13].

Similar behavior was observed for the 1.0 at% of Cr^{3+} sample. However, for the samples with doping above 3.0 at% of Cr^{3+} the zero phonon line is identified between 706 and 708 nm and related to the S2 site. By minimizing the signal at these wavelengths, no zero phonon line remains in the spectra. An explanation for this observation is that at the lower energy region may occur an energy transfer phenomena. As the lower energy absorption region (between 650 and 700 nm) is overlapped to the beginning of the emission region, the Cr^{3+} ion can absorb the energy emitted by Cr^{3+} nearest neighbors.

The vibrational modes for the Cs_2NaAlF_6:Cr^{3+} (0.1%) have been identified in the present work and are given in Tables 2 and 3. Based on the assignment of the vibrational modes of the $[CrF_6]^{3-}$ complex in similar compounds [12,13,38–40,42], the zero phonon line closer mode is identified as the $t_{2u}(\pi)$ asymmetric bending mode, at 14,670 cm^{-1} energy position (for S1 site) and 14,030 cm^{-1} (S2 site), followed by the symmetric $t_{2g}(\pi)$ bending mode at 14,630 cm^{-1} (S1 site) and 14,010 cm^{-1} (S2 site). For hexafluoride complexes the energy value from this transition is very close to its neighbor and its low intensity makes difficult its identification in the vibrational spectra [13]. The next observed mode is the asymmetric bending $t_{1u}(\pi)$ at 14,570 cm^{-1} (S1) and 13,930 cm^{-1} (S2). The first stretching mode, the symmetric $e_g(\sigma)$ is identified at the 14,430 cm^{-1} (S1) and 13,790 cm^{-1} (S2) energies, followed by $a_{1g}(\sigma)$ symmetric mode, at 14,350 cm^{-1}(S1) and 13,710 cm^{-1} (S2). Finally, the stretching asymmetric mode $t_{1u}(\sigma)$ is attributed to the transitions observed at 14,290 cm^{-1} (S1) and 13,690 cm^{-1} (S2).

Assuming that the luminescence temperature quenching is only due to non-radiative decays in low concentration samples,

Table 2
Assignment of the labeled peaks for S1 site with their energies between 672 and 764 nm.

Line	λ (nm)	Energy (cm^{-1})	ΔE (cm^{-1})	Assignment
1	672	14,870	0	Zero phonon line
2	676	14,790	80	Lattice
3	682	14,670	200	$t_{2u}(\pi)$
4	683	14,630	240	$t_{2g}(\pi)$
5	686	14,570	300	$t_{1u}(\pi)$
6	693	14,430	440	$e_g(\sigma)$
7	697	14,350	520	$a_{1g}(\sigma)$
8	700	14,290	580	$t_{1u}(\sigma)$
9	704	14,210	660	$t_{2u}(\pi)+e_g(\sigma)$
10	707	14,150	720	$a_{1g}(\sigma)+t_{2u}(\pi)$
11	709	14,110	760	$t_{2g}(\sigma)+a_{1g}(\sigma)$
12	713	14,030	840	$t_{1u}(\pi)+a_{1g}(\sigma)$
13	725	13,790	1080	$t_{1u}(\sigma)+a_{1g}(\sigma)$
14	736	13,590	1280	$a_{1g}(\sigma)+t_{1u}(\pi)+e_g(\sigma)$
15	749	13,350	1520	$t_{1u}(\sigma)+a_{1g}(\sigma)+e_g(\sigma)$
16	755	13,250	1620	$t_{1u}(\sigma)+2a_{1g}(\sigma)$
17	764	13,090	1780	$2a_{1g}(\sigma)+e_g(\sigma)+t_{1u}(\pi)$

Table 3
Assignment of the labeled peaks for S2 site with their energies between 702 and 807 nm.

Line	λ (nm)	Energy (cm^{-1})	ΔE (cm^{-1})	Assignment
1	702	14,250	0	Zero phonon line
2	705	14,190	60	Lattice
3	709	14,110	140	$t_{2u}(\pi)+C_{3v}$ distortion
4	713	14,030	220	$t_{2u}(\pi)$
5	714	14,010	240	$t_{2g}(\pi)$
6	718	13,930	320	$t_{1u}(\pi)$
7	725	13,790	460	$e_g(\sigma)$
8	729	13,710	540	$a_{1g}(\sigma)$
9	730	13,690	560	$t_{1u}(\sigma)$
10	736	13,590	660	$t_{2u}(\pi)+e_g(\sigma)$
11	741	13,490	760	$t_{1u}(\pi)+e_g(\sigma)$
12	747	13,390	860	$t_{1u}(\pi)+a_{1g}(\sigma)$
13	749	13,350	900	$t_{1u}(\pi)+t_{1u}(\sigma)$
14	755	13,250	1000	$e_g(\sigma)+a_{1g}(\sigma)$
15	760	13,150	1100	$2e_g(\sigma)+t_{2u}(\pi)$
16	767	13,030	1220	$e_g(\sigma)+a_{1g}(\sigma)+t_{2u}(\pi)$
17	772	12,950	1300	$e_g(\sigma)+a_{1g}(\sigma)+t_{1u}(\pi)$
18	778	12,850	1400	$2a_{1g}(\sigma)+t_{1u}(\pi)$
19	781	12,810	1440	$t_{1u}(\pi)+2t_{1u}(\sigma)$
20	787	12,710	1540	$2a_{1g}(\sigma)+e_g(\sigma)$
21	793	12,610	1640	$2a_{1g}(\sigma)+t_{1u}(\sigma)$
22	799	12,510	1740	$t_{1u}(\pi)+3e_g(\sigma)$
23	807	12,390	1860	$2a_{1g}(\sigma)+e_g(\sigma)+t_{1u}(\pi)$

the transition room temperature quantum yield (ϕ) can be estimated from the ratio $\phi=\tau_{300\ K}/\tau_{5\ K}$ [3], where $\tau_{300\ K}$ and $\tau_{5\ K}$ are the radiative lifetime obtained at room and low temperatures, respectively. For the sample with 1.0% of Cr^{3+} doping the obtained radiative lifetime at 300 K is about 312(31) μs and at low temperatures the found value is 397(40) μs, both measured at 754 nm using the phase shift method [43]. At room temperature, these results bring a Cr^{3+} emission quantum yield at about 0.78. The obtained decay time is an average value because at this wavelength there is a contribution in the emission spectra of both sites. The quantum yield for samples with high levels of doping can be not estimated due to the occurrence of transfer energy and non radiative phenomena.

4. Conclusions

Photoluminescence and excitation spectra obtained for single crystals of $Cs_2NaAlF_6:Cr^{3+}$ doped with different concentrations show marked characteristics of Cr^{3+} octahedrically coordinated to F^- ions at 300 K. Such feature is further validated by the low temperature luminescence experiments that exhibited broad spectra with several sharp lines, identified as vibrational transitions due to the $[CrF_6]^{3-}$ octahedral complex. Moreover, the appearance of two zero phonon lines at different energy positions in the 0.1 and 1.0 at% of Cr^{3+} samples can be related to nonequivalent Cr^{3+} octahedral sites. In fact, in the 0.1 at% of Cr^{3+} sample was possible to separate and identify the correspondent emission of both sites, where the higher energy band (at 719 nm) was identified as the site S1 emission, and the lower energy band (779 nm) was assigned to the S2 site emission. These assignments are supported by neutron diffraction, Raman spectroscopy, EPR measurements as well as by ECM calculations [20–22,35]. However, as the concentration increases only the line at lower energy could be observed. Besides, due to the energy transfer phenomena, luminescence quenching, i.e., lowering of the integrated intensity, shift in the luminescence barycenter to lower energy regions as well as decreasing of luminescence lifetime were also observed, implying that the Cr^{3+} ions tend to absorbs the emission generated by his neighbors, and this effect is more pronounced when the doping level increases. In this way, the non-radiative phenonema become more important at high doping levels.

Of more interest is the fact that based on the results presented here, we can infer to the 1.0 at% of Cr^{3+} doped sample a good impurity concentration for the generation of luminescence, due its high quantum yield. Assuming that the emission quantum yield at 5 K is 100%, we obtain a room temperature quantum yield for this sample of about 0.78; in other samples, such as $Be_3Al_2(SiO_3)_6:Cr^{3+}$, this value is about 0.64 [44], in a system similar to the present study, $LiCaAlF_6:Cr^{3+}$ the quantum yield is 0.54 [45], and for the same system studied in the present work, but doped with 0.5% at Cr^{3+} this efficiency is 0.68 [24]. Therefore, this high quantum yield value shows that this system doped with low quantities of impurity ion can be considered an excellent candidate in future applications in lasing devices.

Acknowledgments

SSP, LPS, HNB, RBB and JGDT thank FAPERJ, CAPES, CNPq and FINEP for partial financial support. SSP is grateful to F. Iikawa for the photoluminescence measurements at IFGW-UNICAMP. The authors also thank the referees for improving the paper.

References

[1] D. Deng, H. Ma, S. Xu, Q. Wang, L. Huang, S. Zhao, H. Wang, C. Li, J. Non-Cryst. Solids 357 (2011) 1426.
[2] B. Yasoda, J. Appl. Phys. 98 (2005) 053910.
[3] S. Kück, App. Phys. B: Lasers Opt. 72 (2001) 515.
[4] K. Zheng, D. Zhao, D. Zhang, N. Liu, W. Qin, J. Fluo, Chemistry 132 (2011) 5.
[5] X.L. Duan, D.R. Yuan, L.H. Wang, F.P. Yu, X.F. Cheng, Z.Q. Liu, S.S. Yan, J. Cryst. Growth 296 (2006) 234.
[6] Y. Zhydachevskii, A. Suchocki, M. Berkowski, P. Bilski, S. Warchol, Rad. Meas. 45 (2010) 516.
[7] S. Zhou, G. Feng, B. Wu, N. Jiang, S. Xu, J. Qiu, J. Phys. Chem. C 111 (2007) 7335.
[8] Z.S. Macedo, G.C. Santana, M.C.S. Melo, M.E.G. Valerio, J. Mater. Sci. 42 (2007) 2231.
[9] X. Zhao, X. Wang, B. Chen, Q. Meng, W. Di, G. Ren, Y. Yang, J. Alloy Comp. 433 (2007) 352.
[10] S.S. Pedro, O. Nakamura, R.B. Barthem, L.P. Sosman, J. Fluorine 19 (2009) 211.
[11] M. Yamaga, J.-P.R. Wells, M. Honda, T.P.J. Han, B. Henderson, J. Lumin. 108 (2004) 313.
[12] P. Greenough, A.G. Paulusz, J. Chem. Phys. 70 (1979) 1967.
[13] R.J.M. da Fonseca, L.P. Sosman, A.D. Tavares Jr., H.N. Bordallo, J. Fluorine 10 (2000) 375.
[14] L.P. Sosman, A.D. Tavares Jr, R.J.M. da Fonseca, N.M. Khaidukov, Solid State Commun. 114 (2000) 661.
[15] M.N. Sanz-Ortiz, F. Rodríguez, I. Hernández, R. Valiente, S. Kück, J. Lumin. 128 (2008) 721.
[16] V.F. Zinghenko, J. Fluorine Chem. 131 (2010) 159.
[17] Y. Tanabe, S. Sugano, J. Phys. Soc. Jpn. 9 (1954) 753.
[18] Y. Tanabe, S. Sugano, J. Phys. Soc. Jpn. 9 (1954) 766.
[19] A.S. Marfunin, Physics of Mineral and Inorganic Materials, Springer-Verlag, Berlin, 1979.
[20] C. Rudowicz, M.G. Brik, N.M. Avram, Y.Y. Yeung, P. Gnutek, J. Phys.: Condens. Matter 18 (2006) 5221.
[21] H. Vrielinck, F. Loncke, F. Callens, P. Matthys, N.M. Khaidukov, Phys. Rev. B 70 (2004) 144111[2].
[22] M.G. Brik, N.M. Avram, J. Optoelectron. Adv. Mater. 8 (2006) 102–106.
[23] G.A. Torchia, O. Martinez-Matos, N.M. Khaidukov, J.O. Tocho, Solid State Commun. 130 (2004) 159–163.
[24] G.A. Torchia, D. Schinca, N.M. Khaidukov, J.O. Tocho, Opt. Mater. 20 (2002) 301–304.
[25] G. Meyer, Prog. Solid State Chem. 14 (1982) 141.
[26] D. Babel, R. Haegele, J. Solid State Chem. 18 (1976) 39.
[27] H.N. Bordallo, R.W. Henning, L.P. Sosman, R.J.M. da Fonseca, A.D. Tavares Jr., K.M. Hanif, G.F. Strouse, J. Chem. Phys. 115 (2001) 4300.
[28] E. Fargin, B. Lestienne, J.M. Dance, Solid State Commun. 75 (1990) 769.
[29] A. Trueba, P. Garcia-Fernandez, J.M. García-Lastra, J.A. Aramburu, M.T. Barriuso, M. Moreno, J. Phys. Chem. A 115 (2011) 1423.

[2] Note that the site labeled in the present work as S1 is denoted as M2 in Ref. [21] and the site S2 is denoted as M1 in the same reference.

[30] M.G. Brik, K. Ogasawara, Phys. Rev. B 74 (2006) 045105.
[31] M.T. Barriuso, J.A. Aramburu, M. Moreno, Phys. Status Solidi (b) 196 (1996) 193.
[32] P.A. Tanner, L. Yulong, N.M. Edelstein, K.M. Murdoch, N.M. Khaidukov, J. Phys.: Condens. Matter 9 (1997) 7817.
[33] B. Henderson, G.F. Imbusch, Optical Spectroscopy of Inorganic Solids, Claredon, Oxford, 1989.
[34] S.I. Klokishner, O.V. Kulikova, L.L. Kulyuk, A.A. Nateprov, A.N. Nateprov, S.M. Ostrovsky, A.V. Palii, O.S. Reu, A.V. Siminel, Opt. Mater. 31 (2008) 284.
[35] L.P. Sosman, F. Yokaichiya, H.N. Bordallo, J. Magn. Magn. Mater. 321 (2009) 2210.
[36] B. Henderson, R.H. Bartram, Crystal-Field Engineering of Solid State Laser Materials, Cambridge University Press, 2000.
[37] Z. Zhang, K.T.V. Gratan, A.W. Palmer, Phys. Rev. B 48 (1993) 7772.
[38] B. Villacampa, R. Cases, R. Alcalá, J. Lumin. 63 (1995) 289.
[39] G.R. Wein, D.S. Hamilton, U. Sliwczuk, A.G. Rinzler, R.H. Bartram, J. Phys.: Condens. Matter 13 (2001) 2363.
[40] M.A.F.M. Silva, R.B. Barthem, L.P. Sosman, J. Solid State Chem. 179 (2006) 3718.
[41] T. Abritta, F.S. Barros, J.T. Melamed, J. Lumin. 33 (1985) 141.
[42] L.P. Sosman, R.J.M. Fonseca, A.D. Tavares Jr., M.K.K. Nakaema, H.N. Bordallo, J. Fluorine 16 (2006) 317.
[43] J.E. Martin, L.E. Shea-Rohwer, J. Lumin. 121 (2006) 573.
[44] M.L. Shand, S.T. Lai, IEEE J. Quantum Electron. 20 (1984) 105.
[45] J.A. Caird, S.A. Payne, P.R. Staver, A.J. Ramponi, L.L. Chase, W.F. Krupke, IEEE J. Quantum Electron. 24 (1992) 1077.